

Infinite ergodic theory for three heterogeneous stochastic models with application to subrecoil laser cooling

Takuma Akimoto,^{1,*} Eli Barkai,² and Günter Radons³

¹*Department of Physics, Tokyo University of Science, Noda, Chiba 278-8510, Japan*

²*Department of Physics, Bar-Ilan University, Ramat-Gan 5290002, Israel*

³*Institute of Physics, Chemnitz University of Technology, 09107 Chemnitz, Germany*

(Dated: February 2, 2022)

We compare ergodic properties of the kinetic energy for three stochastic models of subrecoil-laser-cooled gases. One model is based on a heterogeneous random walk (HRW), another is an HRW with long-range jumps (the exponential model), and the other is a mean-field-like approximation of the exponential model (the deterministic model). All the models show an accumulation of the momentum at zero in the long-time limit, and a formal steady state cannot be normalized, i.e., there exists an infinite invariant density. We obtain the exact form of the infinite invariant density and the scaling function for the exponential and deterministic models and devise a useful approximation for the momentum distribution in the HRW model. While the models are kinetically non-identical, it is natural to wonder whether their ergodic properties share common traits, given that they are all described by an infinite invariant density. We show that the answer to this question depends on the type of observable under study. If the observable is integrable, the ergodic properties such as the statistical behavior of the time averages are universal as they are described by the Darling-Kac theorem. In contrast, for non-integrable observables, the models in general exhibit non-identical statistical laws. This implies that focusing on non-integrable observables, we discover non-universal features of the cooling process, that hopefully can lead to a better understanding of the particular model most suitable for a statistical description of the process. This result is expected to hold true for many other systems, beyond laser cooling.

I. INTRODUCTION

In many cases in equilibrium statistical physics, a steady-state solution of a master equation yields the equilibrium distribution. However, the formal steady-state solution may not be normalizable, especially for non-stationary stochastic processes found in the context of anomalous diffusion and non-normalizable Boltzmann states [1–10]. Such an unnormalized formal steady state is called an infinite invariant density, which is known from deterministic dynamical systems [11, 12]. Interestingly, dynamical systems with infinite invariant densities exhibit non-stationary behaviors and trajectory-to-trajectory fluctuations of time averages, whereas they are ergodic in the mathematical sense [12].

The ergodic properties of dynamical systems with infinite invariant densities have been established in infinite ergodic theory [12–18], where distributional limit theorems for time-averaged quantities play an important role. The distributional limit theorems state that time-averaged observables obtained with single trajectories show trajectory-to-trajectory fluctuations. The distribution function of the fluctuations depends on whether the observable is integrable with respect to the infinite invariant measure [15, 16, 19–21]. This distributional behavior of time averages is a characteristic feature of infinite ergodic theory. Similar distributional behaviors have been observed in experiments such as the fluorescence of

quantum dots, diffusion in living cells, and interface fluctuations in liquid crystals [22–29].

Subrecoil laser cooling is a powerful technique for cooling atoms [30, 31]. A key idea of this technique is to realize experimentally a heterogeneous random walk (HRW) of the atoms in momentum space. In a standard cooling technique such as Doppler cooling, a biased random walk is utilized to shift the momenta of atoms towards zero [30]. Thus, Doppler cooling is routinely modeled using a standard Fokker–Planck equation for the momentum distribution. In contrast to a homogeneous random walk, an HRW enables the accumulation of walkers at some point without an external force induced by the Doppler effect. In other words, the probability of finding a random walker at that point converges to one in the long-time limit due to an ingenious trapping mechanism, that gives rise to a heterogeneous environment. Hence, for subrecoil laser cooling, instead of a biased random walk, an HRW plays an essential role. This was a paradigm shift for cooling and useful for cooling beyond the lowest limit obtained previously in standard cooling techniques [30].

It is now well recognized that infinite ergodic theory provides a fundamental theory for subrecoil-laser cooling [32]. In [33] three models of subrecoil laser cooling are proposed. One is based on the HRW, another is obtained from the HRW model with long-range jumps called the exponential model, and the third is a mean-field-like approximation of the exponential model called the deterministic model. It is known that the infinite density depends in principle on some details of the system [7–9]. The question then remains: what elements of the infinite

* takuma@rs.tus.ac.jp

ergodic theory remain universal? These questions with respect to the general validity of the theory are particularly important because we have at least two general classes of observables, i.e., integrable and non-integrable with respect to the infinite invariant measure. To unravel the universal features of subrecoil laser cooling, we explore here the three models of subrecoil laser cooling.

The rest of the paper is organized as follows. In Sec. II, we introduce the three stochastic models of subrecoil laser cooling. In Sec. III, we introduce the master equation and the formal steady-state solution, i.e., the infinite invariant density, in the HRW model. In Sections IV and V, we present the infinite invariant densities and the distributional limit theorems for the time average of the kinetic energy in the deterministic and exponential model, respectively. While the master equations for the HRW and exponential model are different, we show that the propagators and the distributional behaviors of the time-averaged kinetic energy match very well. Section VI is devoted to the conclusion. In the Appendix, we give a derivation of the moments of the associated action as a function of time t .

II. THREE STOCHASTIC MODELS

Here, we introduce the three stochastic models of subrecoil laser cooling. All the models describe stochastic dynamics of the momentum of an atom.

First, the HRW model is a one-dimensional continuous-time random walk (CTRW) in momentum space. The CTRW is a random walk with continuous waiting times. Usually, in the CTRW the waiting times are independent and identically distributed (IID). In the HRW model, they are not an IID random variable. In the HRW, the waiting time between stochastic updates of momentum given p is exponentially distributed with a mean waiting time $1/R(p)$. After waiting the atom jolts and momentum is modified. We assume that the jump distribution follows a Gaussian distribution:

$$G(\Delta p) = (2\pi\sigma^2)^{-1/2} \exp[-\Delta p^2/(2\sigma^2)], \quad (1)$$

where Δp is a jump of the momentum of an atom and σ^2 is the variance of the jumps. The heterogeneous rate $R(p)$ is important to cool atoms and can be realized by velocity selective coherent population trapping in experiments [34]. In subrecoil laser cooling, the jump rate $R(p)$ is typically given by

$$R(p) \propto |p|^\alpha \quad (2)$$

for $|p| \rightarrow 0$ [33], where α is a positive constant. This constant can take any value in principle [35], for instance, $\alpha = 2$ in velocity-selective coherent population trapping [34]. In what follows, we consider a specific jump rate:

$$R(p) = \begin{cases} c^{-1}|p|^\alpha & (|p| < p_0) \\ c^{-1}|p_0|^\alpha & (|p| \geq p_0), \end{cases} \quad (3)$$

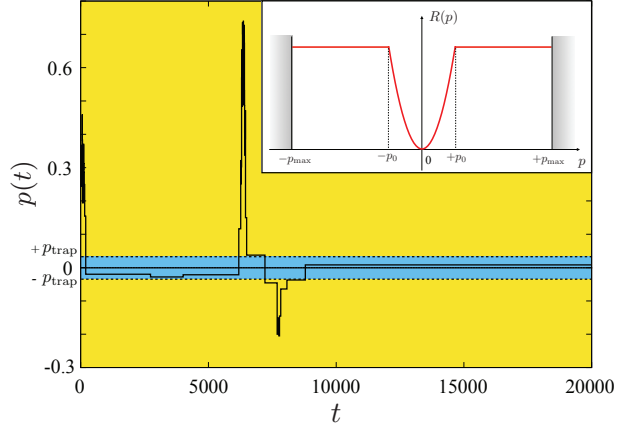


FIG. 1. A typical trajectory of momentum $p(t)$ in the HRW model, where $R(p) = |p|^2$, $p_0 = 1$, $p_{\max} = 2$, $\sigma^2 = 0.01$, and $p_{\text{trap}} \cong 0.035$ is shown for reference. The blue and the yellow region are the trapping and the recycling region, respectively. The inset is a schematic illustration of the jump rate $R(p)$.

where p_0 is the width of the jump rate dip and c is a positive constant (see Fig. 1). A typical trajectory in the HRW model is shown in Fig. 1. Since the HRW model is a non-biased random walk, the momentum will eventually reach high values. To prevent such a situation, one considers a confinement in an experimentally realizable way.

Next, we explain how we obtain the other two models, i.e., the exponential and the deterministic model, based on the HRW model. The region in momentum space can be divided into two regions, i.e., trapping and recycling region [33]. The trapping region is defined as $|p| \leq p_{\text{trap}}$, where $p_{\text{trap}} \ll \sigma$. In the recycling region, the atom undergoes a non-biased random walk, which will eventually lead the atom back to the trapping region with the aid of the confinement. In the HRW model, the trap size p_{trap} does not play any role. However, the jump of a random walker is long-ranged in the trapping region in the sense that momentum after jumping in the trapping region is approximately independent of the previous momentum. Therefore, the following assumption is quite reasonable. In the exponential and the deterministic model, momentum after jumping in the trapping region is assumed to be an IID random variable. In particular, the probability density function (PDF) $\chi(p)$ for the momentum at every jump in the trapping region is assumed to be uniform:

$$\chi(p) = \frac{1}{2p_{\text{trap}}} \quad \text{for } p \in [-p_{\text{trap}}, p_{\text{trap}}]. \quad (4)$$

A trajectory for the exponential model is similar to that for the HRW model. However, a crucial difference between the HRW model and the exponential model is in the nature of the waiting time: the waiting time is an independent random variable in the exponential model, whereas it is not in the HRW model. In the HRW model, the waiting time is not independent of the previous wait-

ing time because the momentum depends on the previous one. Such a dependence of waiting times is also the nature of the quenched trap model (QTM), which is a random walk in a static random heterogeneous environment [37]. Note that the heterogeneous environment in the HRW model is static but not random.

A difference between the exponential and the deterministic models is in the coupling between the waiting time and the momentum. In the exponential model, momentum and waiting time are stochastically coupled. As for the HRW this model is a Markov model and the conditional PDF of the waiting time given the momentum p follows an exponential distribution with mean $1/R(p)$. On the other hand, the deterministic model is a non-Markov model. The waiting time given the momentum p is deterministically prescribed as $\tau(p) = 1/R(p)$ [33]. In other words, the waiting time, which is a random variable in the exponential model, is replaced by its mean in the deterministic model. In this sense, the deterministic model is a mean-field-like model of the exponential model. Note that this implies a double meaning of $1/R(p)$: while in the HRW and in the exponential model it is the mean waiting time, whereas in the deterministic model it is the exact waiting time for a given momentum p .

III. HETEROGENEOUS RANDOM WALK MODEL

Here, we consider the HRW model confined to the interval $[-p_{\max}, p_{\max}]$ [31, 34]. The momentum $p(t)$ at time t undergoes a non-biased random walk. Jumps of the momentum are attributed to photon scattering and spontaneous emissions. Importantly, its jump rate $R(p)$ follows Eq. (3) for $|p| < p_0$. In particular, we consider that the jump rate follows Eq. (3) [31]. In this model, the conditional PDF $q(\tilde{\tau}|p)$ of $\tilde{\tau}$ given p follows the exponential distribution:

$$q(\tilde{\tau}|p) = R(p) \exp(-R(p)\tilde{\tau}). \quad (5)$$

Clearly, the mean waiting time given p explicitly depends on p when $|p| < p_0$. Thus, the random walk is heterogeneous. A confinement of atoms can also be achieved by Doppler cooling [30, 31]. However, for simplicity, we consider reflecting boundary conditions at $p = \pm p_{\max}$. As will be observed later, the size of the confinement or the width of the jump rate dip does not affect the asymptotic behavior of the scaling function of the propagator. More precisely, the scaling function and fluctuations of the time-averaged energy do not depend on p_{\max} and p_0 . As shown in Fig. 1, the momentum of an atom remains constant for a long time when $|p|$ is small. On the other hand, momentum changes frequently occur when $|p|$ is away from zero.

A. Master equation and infinite invariant density

The time evolution of the probability density function (PDF) $\rho(p, t)$ of momentum p at time t is given by the master equation with gain and loss terms:

$$\frac{\partial \rho(p, t)}{\partial t} = \int_{-p_{\max}}^{p_{\max}} dp' [W(p' \rightarrow p)\rho(p', t) - W(p \rightarrow p')\rho(p, t)], \quad (6)$$

where $W(p \rightarrow p')$ is the transition rate from p to p' . Jump and transition rates can be represented as

$$R(p) = \int_{-\infty}^{\infty} dp' W(p \rightarrow p') \quad (7)$$

and

$$W(p \rightarrow p') = R(p)G(p'|p), \quad (8)$$

where $G(p'|p)$ is the conditional PDF of p' given p , respectively, where both the domain and the codomain of the function $G(p'|p)$ are $[-p_{\max}, p_{\max}]$ because of the confinement. Note that $G(p'|p)$ cannot depend solely on the difference $p' - p$ when a random walker reaches the reflecting boundary, i.e., $|p' + \Delta p| > p_{\max}$, where Δp is a jump length. It follows that the master equation (Eq. (6)) of the HRW model takes the following form:

$$\frac{\partial \rho(p, t)}{\partial t} = -R(p)\rho(p, t) + \int_{-p_{\max}}^{p_{\max}} dp' \rho(p', t) R(p')G(p|p'). \quad (9)$$

The stationary solution $\rho^*(p)$ is easily obtained from the detailed balance in Eq. (6), i.e.,

$$W(p' \rightarrow p)\rho^*(p') - W(p \rightarrow p')\rho^*(p) = 0, \quad (10)$$

where $\rho^*(p)$ is the stationary solution. For $|p|$ and $|p'| \ll p_{\max}$, the conditional PDF $G(p|p')$ is approximately symmetric, i.e., $G(p|p') = G(p'|p)$. Therefore, for $|p|, |p'| \ll p_{\max}$, detailed balance yields

$$R(p')\rho^*(p') = R(p)\rho^*(p), \quad (11)$$

which is fulfilled only if $R(p)\rho^*(p)$ is constant. In subrecoil laser cooling, the jump rate $R(p)$ becomes a power-law form near $p \cong 0$, i.e., Eq. (2). For example, the velocity selective coherent population trapping gives $\alpha = 2$ [34], and the Raman cooling experiments realize $\alpha = 2$ and 4 by 1D square pulses and the Blackman pulses, respectively [36]. Therefore, for $|p| \ll p_{\max}$, the steady-state distribution $\rho^*(p)$ is formally given by

$$\rho^*(p) = \text{const.}/R(p) \propto |p|^{-\alpha}. \quad (12)$$

For $\alpha \geq 1$, it cannot be normalized because of the divergence at $p = 0$, and $\rho^*(p)$ is therefore called an infinite invariant density. Although $\rho^*(p)$ is the formal steady state, a steady state in the conventional sense does not exist in the system with $\alpha \geq 1$. As will be shown below, a part of the infinite invariant density can be observed

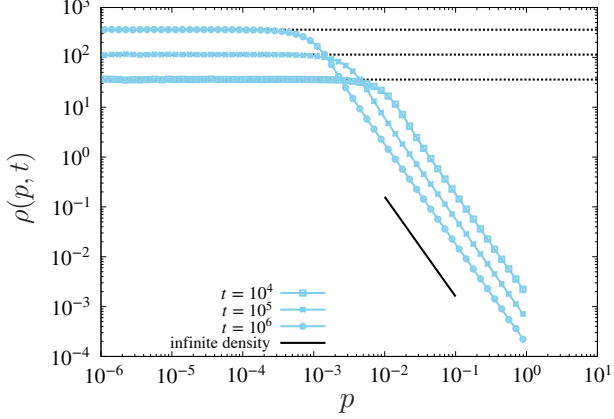


FIG. 2. Time evolution of the propagator in the HRW model ($p_0 = p_{\max} = 1$, $\sigma = 1$, and $R(p) = |p|^2$). Symbols with lines are the numerical results of the HRW model by simulating trajectories of random walkers. The solid line represents a part of a steady-state solution, $\rho^*(p) \propto |p|^{-\alpha}$, for reference. The dashed lines represent plateaus around $|p| = 0$, which shift up with time t . Initial momentum is chosen uniformly on $[-1, 1]$.

in the propagator especially for a large time. Moreover, it will be shown that $t^{1-1/\alpha} \rho(p, t)$ converges to the infinite invariant density for $t \rightarrow \infty$. Therefore, the infinite invariant density is not a vague solution but plays an important role in reality.

Figure 2 shows numerical simulations of the propagator in the HRW model. The propagator accumulates near zero, and $\rho(p, t)$ around $p \cong 0$ increases with time t . Moreover, a power-law form, i.e., $p^{-\alpha}$, of the formal steady state $\rho^*(p)$ is observed, especially when t is large, except for $p \cong 0$ (see also Fig. 3). Since the infinite invariant density $\rho^*(p)$ cannot be normalized, the propagator never converges to $\rho^*(p)$.

IV. EXPONENTIAL MODEL

In this section, we give theoretical results for the exponential model, which were already shown in our previous study [32]. Here, we consider the Laplace transform of the propagator and execute the inverse transform to obtain the infinite invariant density and the scaling function. The derivation of the scaling function is different from the previous study [32], where the master equation is directly solved.

A. Master equation, infinite invariant density, and scaling function

In the exponential model, the jump distribution is independent of the previous momentum unlike the HRW model. It follows that the transition rate of the exponen-

tial model becomes

$$W(p \rightarrow p') = R(p)\chi(p'). \quad (13)$$

It follows that the master equation of the exponential model becomes

$$\frac{\partial \rho(p, t)}{\partial t} = -R(p)\rho(p, t) + \frac{1}{2p_{\text{trap}}} \int_{-p_{\text{trap}}}^{p_{\text{trap}}} R(p')\rho(p', t)dp'. \quad (14)$$

The second term, i.e., gain term, is different from that in the HRW model, Eq. (9).

In the exponential model, the momentum remains constant until the next jump, and the conditional waiting time distribution given by momentum p follows an exponential distribution with mean $1/R(p)$, which is the same as in the HRW model, i.e., Eq. (5). Because the conditional waiting time distribution depends on p , the joint PDF of momentum p and waiting time $\tilde{\tau}$,

$$\phi(p, \tilde{\tau}) = \langle \delta(p - p_i) \delta(\tilde{\tau} - \tilde{\tau}_i) \rangle, \quad (15)$$

where $\delta(\cdot)$ is the δ function, plays an important role. It can be expressed by

$$\phi(p, \tilde{\tau}) = q(\tilde{\tau}|p)\chi(p), \quad (16)$$

where $q(\tilde{\tau}|p)$ is the conditional PDF $q(\tilde{\tau}|p)$ of waiting time $\tilde{\tau}$ given p , Eq.(5), and $\chi(p)$ is given by Eq.(4)

The unconditioned PDF of the waiting time is given by

$$\psi(\tilde{\tau}) = \frac{1}{2p_{\text{trap}}} \int_{-p_{\text{trap}}}^{p_{\text{trap}}} R(p) \exp(-R(p)\tilde{\tau})dp, \quad (17)$$

which follows from averaging the joint PDF, over a uniform density, i.e., $\chi(p)$. By a change of variables ($y = R(p)\tilde{\tau}$), we have

$$\psi(\tilde{\tau}) = \frac{c^{\frac{1}{\alpha}} \tilde{\tau}^{-1-\frac{1}{\alpha}}}{\alpha p_{\text{trap}}} \int_0^{\tilde{\tau} c^{-1} p_{\text{trap}}^{\alpha}} y^{\frac{1}{\alpha}} \exp(-y) dy \quad (18)$$

$$\sim \frac{\gamma c^{\gamma} \Gamma(1+\gamma)}{p_{\text{trap}}} \tilde{\tau}^{-1-\gamma} \quad (\tilde{\tau} \rightarrow \infty), \quad (19)$$

where $\gamma = 1/\alpha$. In what follows, we assume $\gamma \leq 1$, which implies that the mean waiting time diverges. Therefore, as will be shown, the dynamics of p becomes non-stationary.

The exponential model is a continuous-time Markov chain, which is a special type of semi-Markov process (SMP). Therefore, we utilize an SMP with continuous variables to obtain analytical results for the exponential model. In the SMP, the state value is determined by the waiting time, which is randomly selected, or equivalently, the waiting time is determined by the state value, which is randomly chosen. In the latter case, the state value is renewed according to the PDF $\chi(p)$. In general, an SMP is characterized by the state distribution $\chi(p)$ and the joint PDF of the state value and the waiting time $\phi(p, \tau)$, Eq. (16). The deterministic model, which we will treat in

Sect. V, is identical to the SMP with a deterministic coupling between the state value and the waiting time. On the other hand, the SMP with an exponential conditional PDF of waiting times given the state is equivalent to the exponential model. For the SMP with $\chi(p)$ and $\phi(p, \tau)$, the Laplace transform of the propagator with respect to t is obtained as in Ref. [38]. Applying the result to the exponential model yields

$$\hat{\rho}(p, s) = \frac{1}{s} \frac{\chi(p) - \hat{\phi}(p, s)}{1 - \hat{\psi}(s)}, \quad (20)$$

where $\hat{\phi}(p, s)$ and $\hat{\psi}(s)$ are the Laplace transforms of $\phi(p, \tilde{\tau})$ and $\psi(\tilde{\tau})$ with respect to $\tilde{\tau}$, respectively. Here, the ordinary renewal process was used as the initial condition [38, 39].

In the exponential model, the Laplace transform of the joint PDF is given by

$$\hat{\phi}(p, s) = \frac{\chi(p)R(p)}{s + R(p)}. \quad (21)$$

It follows from Eqs. (20) and (21) that $\hat{\rho}(p, s)$ becomes

$$\hat{\rho}(p, s) = \frac{\chi(p)}{s + R(p)} \frac{1}{1 - \hat{\psi}(s)}. \quad (22)$$

In the long-time limit ($s \rightarrow 0$), it becomes

$$\hat{\rho}(p, s) \cong \frac{1}{s + c^{-1}|p|^\alpha} \frac{1}{2\Gamma(1 - \alpha^{-1})\Gamma(1 + \alpha^{-1})(cs)^{\alpha^{-1}}}, \quad (23)$$

where $\chi(p) = 1/(2p_{\text{trap}})$ is used. Interestingly, the Laplace transform of the propagator does not depend on p_{trap} . To obtain the exponential model from the HRW model, we assumed that p_{trap} is much smaller than σ . However, the asymptotic behavior of the propagator is independent of p_{trap} in the exponential model. Therefore, p_{trap} can be assumed to be $p_{\text{trap}} \ll \sigma$ without loss of generality when we consider the asymptotic behavior of the propagator. In other words, the exponential model with the uniform approximation for $\chi(p)$ is a good approximation for the HRW model. By the inverse Laplace transform, we have

$$\rho(p, t) \cong \frac{\sin(\pi\alpha^{-1})}{2\pi c^{\alpha^{-1}}\Gamma(1 + \alpha^{-1})} \int_0^t dt' e^{-c^{-1}|p|^\alpha(t-t')} t'^{\alpha^{-1}-1} \quad (24)$$

for $t \rightarrow \infty$. Through a change of variables ($u = t'/t$), we obtain

$$\rho(p, t) \cong \frac{\sin(\pi\alpha^{-1})t^{\alpha^{-1}}}{2\pi c^{\alpha^{-1}}\Gamma(1 + \alpha^{-1})} \int_0^1 du e^{-c^{-1}|p|^\alpha t(1-u)} u^{\alpha^{-1}-1}. \quad (25)$$

Therefore, the cooled peak, i.e., $\rho(0, t)$, increases with $t^{\alpha^{-1}}$, which means that the probability of finding the cooled state ($p \cong 0$) increases with time, i.e., this is a signature of cooling.

For $|p| > 0$ and $t \gg 1$, the integral is approximated as

$$\rho(p, t) \cong \frac{\sin(\pi\alpha^{-1})t^{\alpha^{-1}-1}}{2\pi c^{\alpha^{-1}-1}\Gamma(1 + \alpha^{-1})} \frac{1}{|p|^\alpha}. \quad (26)$$

Furthermore, an infinite invariant density is obtained as

$$\lim_{t \rightarrow \infty} t^{1-\alpha^{-1}} \rho(p, t) = I_{\text{exp}}(p) \equiv \frac{\sin(\pi\alpha^{-1})|p|^{-\alpha}}{2\pi c^{\alpha^{-1}-1}\Gamma(1 + \alpha^{-1})} \quad (27)$$

for $|p| \leq p_{\text{trap}}$. The power-law form of Eq. (27), $I_{\text{exp}}(p) \propto |p|^{-\alpha}$, in the exponential model matches with the infinite invariant density, Eq. (12), in the HRW model.

Through a change of variables ($p' = t^{\alpha^{-1}}p/c^{\alpha^{-1}}$), we obtain the rescaled propagator $\rho_{\text{res}}(p', t)$. In the long-time limit, the rescaled propagator converges to a time-independent function $g_{\text{exp}}(p')$ (scaling function):

$$\rho_{\text{res}}(p', t) \equiv \rho(c^{\alpha^{-1}}p'/t^{\alpha^{-1}}, t) \left| \frac{dp}{dp'} \right| \rightarrow g_{\text{exp}}(p'), \quad (28)$$

where the scaling function is given by

$$g_{\text{exp}}(p') \equiv \frac{\sin(\pi\alpha^{-1})}{2\pi\Gamma(1 + \alpha^{-1})} \int_0^1 du e^{-|p'|^\alpha(1-u)} u^{\alpha^{-1}-1}. \quad (29)$$

This scaling function describes the propagator near $p = 0$. This result was previously obtained by a different approach [32].

Here, we are going to demonstrate that the theory of the exponential model describes the asymptotic behavior of the propagator in the HRW model surprisingly well. Figure 3 shows that the propagator for the HRW model is in perfect agreement with the analytical result of the exponential model, i.e., Eq. (25). In the numerical simulations of the HRW model, we generated 10^8 trajectories to obtain the propagator. There are two forms in the propagator. The propagator near $p = 0$ increases with time t . On the other hand, the propagator for $p > 0$ asymptotically approaches a power-law form, i.e., the infinite invariant density. Figure 4 shows that the rescaled propagator of the HRW model for different times is well captured by the scaling function $g_{\text{exp}}(p')$ without fitting parameters, where we generated 10^8 trajectories to obtain the rescaled propagator. Because the scaling function describes the details of the propagator near $p = 0$ and is universal in the sense that it does not depend on p_{trap} in the exponential model, the dynamics of the HRW model near $p = 0$ should also be universal and does not depend on the details of the jump distribution $G(\Delta p)$. In fact, as shown in Fig. 4, the rescaled propagator does not depend on σ^2 . This is one of the reasons why the uniform approximation works very well. Moreover, because the momentum almost certainly approaches zero in the long-time limit, the assumption of $|p| \ll 1$ is correct for $t \gg 1$. Furthermore, it can be confirmed that Eq. (25) becomes a solution to the master equation, Eq. (9), in the long-time limit, where the momentum at every jump is approximately renewed according to $G(\Delta p)$. Therefore,

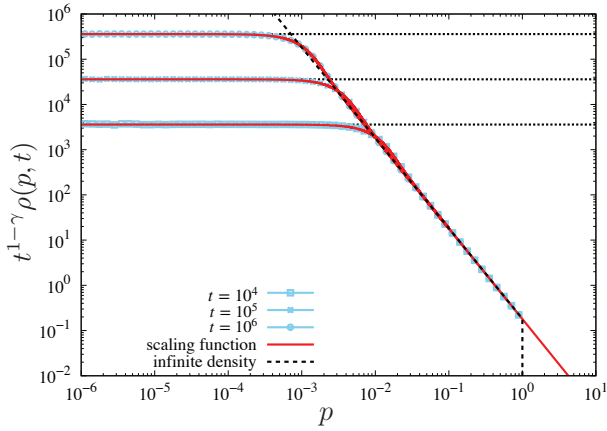


FIG. 3. Time evolution of the propagator, i.e. data from Fig. 2, multiplied by $t^{1-\gamma}$ in the HRW model for different times ($\alpha = 2$, $c = 1$, $p_0 = p_{\max} = 1$, and $\sigma^2 = 1$). Symbols with lines are the results of numerical simulations for the HRW model. The dashed lines represent the infinite density, i.e., Eq. (27). The solid lines represent rescaled scaling functions, $t g_{\exp}(t^\gamma p)$. The dotted lines represent $t g_{\exp}(0)$ for different values of t . The initial momentum is chosen uniformly on $[-1, 1]$.

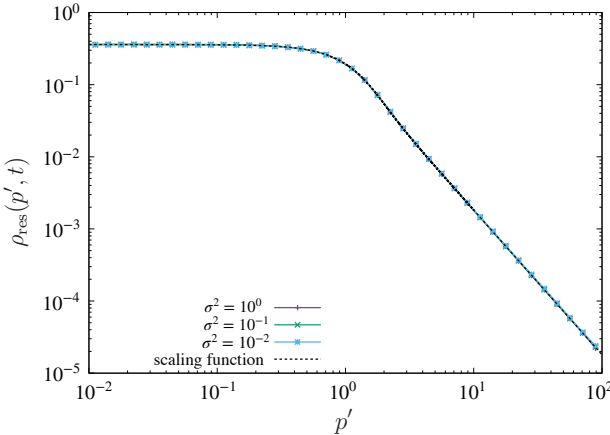


FIG. 4. Rescaled propagator of the HRW model for different values of σ^2 ($\alpha = 2$, $c = 1$, $p_0 = p_{\max} = 1$, and $t = 10^4$). Symbols with lines are the results of numerical simulations for the HRW model. The dashed solid line represents the scaling function, i.e., Eq. (29). The initial position is chosen uniformly on $[-1, 1]$. Note that the results for different σ^2 are indistinguishable.

the theory of the exponential well describes the propagator for the HRW model.

B. Ensemble and time averages of observables

In this subsection, we consider the ensemble average of an observable, which is defined as

$$\langle \mathcal{O}(p(t)) \rangle \equiv \int_{-p_{\text{trap}}}^{p_{\text{trap}}} \mathcal{O}(p) \rho(p, t) dp. \quad (30)$$

We assume that the observable is $\mathcal{O}(p) = C|p|^\beta$ and $\beta > -1$. For example, if $\beta = 2$ we are considering the kinetic energy of atom. Through a change of variables ($p' = t^{\alpha-1} p / c^{\alpha-1}$) and using the scaling function, Eq. (29), we have

$$\langle \mathcal{O}(p(t)) \rangle \sim \int_{-(\frac{t}{c})^{\alpha-1} p_{\text{trap}}}^{(\frac{t}{c})^{\alpha-1} p_{\text{trap}}} \mathcal{O}\left(\frac{c^{\alpha-1} p'}{t^{\alpha-1}}\right) g_{\exp}(p') dp' \quad (31)$$

for $t \rightarrow \infty$.

When $|p|^\beta$ is integrable with respect to $g_{\exp}(p)$, i.e., $\int_{-\infty}^{\infty} g_{\exp}(p) |p|^\beta dp < \infty$, β satisfies $-1 < \beta < \alpha - 1$. In this case, the asymptotic behavior of the ensemble average becomes

$$\langle \mathcal{O}(p(t)) \rangle \sim \frac{C c^{\beta \alpha^{-1}}}{t^{\beta \alpha^{-1}}} \int_{-\infty}^{\infty} |p'|^\beta g_{\exp}(p') dp' \quad (t \rightarrow \infty). \quad (32)$$

On the other hand, when $|p|^\beta$ is integrable with respect to $I_{\exp}(p)$, i.e., $\int_{-p_{\text{trap}}}^{p_{\text{trap}}} I_{\exp}(p) \mathcal{O}(p) dp < \infty$, β satisfies $\beta > \alpha - 1$ (> 0), implying that $|p|^\beta$ is not integrable with respect to the scaling function, i.e., $\int_{-\infty}^{\infty} g_{\exp}(p) |p|^\beta dp = \infty$. In this case, the asymptotic behavior of the ensemble average becomes

$$\langle \mathcal{O}(p(t)) \rangle \sim t^{\alpha^{-1}-1} \int_{-p_{\text{trap}}}^{p_{\text{trap}}} I_{\exp}(p) \mathcal{O}(p) dp \quad (t \rightarrow \infty). \quad (33)$$

Therefore, the asymptotic behavior becomes

$$\langle \mathcal{O}(p(t)) \rangle \propto t^{-\lambda(\alpha, \beta)} \quad (t \rightarrow \infty), \quad (34)$$

and the integrability of the observable with respect to the scaling function or infinite invariant density determines the power-law exponent $\lambda(\alpha, \beta)$. In the case of $\beta = \alpha - 1$, the integrals of the observable with respect to both the scaling function and infinite invariant density diverge. In this case, the integration in Eq. (31) contains a logarithmic divergence for $t \rightarrow \infty$. Therefore, the leading order for $t \rightarrow \infty$ is

$$\langle \mathcal{O}(p(t)) \rangle \propto t^{\alpha^{-1}-1} \ln t. \quad (35)$$

The power-law exponent $\lambda(\alpha, \beta)$ in the exponential model is given by

$$\lambda(\alpha, \beta) = \begin{cases} 1 - \alpha^{-1} & (\beta > \alpha - 1) \\ \beta \alpha^{-1} & (\beta < \alpha - 1). \end{cases} \quad (36)$$

As will be shown later, the decay process is universal in the sense that $\lambda(\alpha, \beta)$ does not depend on the three

models that we consider here. Moreover, the fastest decay, which implies the maximum of $\lambda(\alpha, \beta)$, is realized at the transition point between integrable and non-integrable with respect to the infinite invariant measure, i.e., $\alpha = \beta + 1$. In particular, the fastest decay of the kinetic energy, i.e., $\beta = 2$, can be achieved for $\alpha = 3$, which suggests that the cooling efficiency, in a sense, is optimized at this point. As shown in the previous subsection, the height of the cooled peak increases with $t^{\alpha^{-1}}$. Moreover, the half-width of the cooled peak in the momentum distribution decays with $t^{-\alpha^{-1}}$. If we use the half-width of the cooled peak in the momentum distribution to characterize the cooling efficiency, the optimized parameter is $\alpha = 1$. Therefore, the most efficient cooling parameter depends on the definition of efficiency.

C. Distributional characteristics of time-averaged observables

Here, we construct a theory of the distribution of time averages in the exponential model. The time average of an observable $\mathcal{O}(p)$ is defined by

$$\overline{\mathcal{O}}(t) \equiv \frac{1}{t} \int_0^t \mathcal{O}(p(t')) dt'. \quad (37)$$

We obtain the mean and variance for two cases, when the observable is integrable with respect to the infinite density and when it is not. In what follows, we consider kinetic energy as a specific example, i.e., $\mathcal{O}(p) = p^2$. The integrated value of an observable $\mathcal{O}(p)$ denoted by $\mathcal{S}(t)$ can be represented by

$$\mathcal{S}(t) = \int_0^t \mathcal{O}(p(t')) dt' \quad (38)$$

$$= \sum_{i=1}^{N(t)} \Delta \mathcal{S}_i + \mathcal{O}(p_{N(t)+1})(t - t_{N(t)}), \quad (39)$$

where $\Delta \mathcal{S}_i = \mathcal{O}(p_i) \tilde{\tau}_i$, $N(t)$ is the number of jumps until time t , p_i is the momentum during $[t_{i-1}, t_i]$, and $t_i = \tilde{\tau}_1 + \dots + \tilde{\tau}_i$. The integrated value $\mathcal{S}(t)$ is a piecewise linear function of t [32] because $\mathcal{O}(p(t))$ is a piecewise constant function, where p_i and $\tilde{\tau}_i$ are coupled stochastically. The joint PDF of $\Delta \mathcal{S}_i$, $\tilde{\tau}_i$, and p_i denoted by $\phi_3(x, \tilde{\tau}, p)$ is given by

$$\phi_3(x, \tilde{\tau}, p) = \chi(p) R(p) e^{-R(p)\tilde{\tau}} \delta(x - \mathcal{O}(p)\tilde{\tau}). \quad (40)$$

The joint PDF of the integrated value of an elementary step and the waiting time $\tilde{\tau}$ is given by

$$\begin{aligned} \phi_2(x, \tilde{\tau}) &= \int_{-p_{\text{trap}}}^{p_{\text{trap}}} dp \phi_3(x, \tilde{\tau}, p) \\ &= \frac{1}{2p_{\text{trap}}\sqrt{x\tilde{\tau}}} R(\sqrt{x/\tilde{\tau}}) e^{-R(\sqrt{x/\tilde{\tau}})\tilde{\tau}} \quad (\sqrt{x/\tilde{\tau}} < p_{\text{trap}}). \end{aligned}$$

Let $Q(x, t)$ be the PDF of $x = \mathcal{S}(t)$ when a jump occurs exactly at time t ; then, we have

$$Q(x, t) = \int_0^x dx' \int_0^t dt' \phi_t(x', t') Q(x - x', t - t') + Q_0(x, t), \quad (41)$$

where $Q_0(x, t) = \delta(x)\delta(t)$. The PDF of $\mathcal{S}(t)$ at time t is given by

$$P(x, t) = \int_0^x dx' \int_0^t dt' \Phi_2(x', t') Q(x - x', t - t'), \quad (42)$$

where

$$\Phi_2(x, t) = \int_t^\infty d\tilde{\tau} \int_{-p_{\text{trap}}}^{p_{\text{trap}}} dp \chi(p) R(p) e^{-R(p)\tilde{\tau}} \delta(x - \mathcal{O}(p)\tilde{\tau}). \quad (43)$$

The double-Laplace transform with respect to x and t ($u \leftrightarrow x$ and $s \leftrightarrow t$) yields

$$\widehat{P}(u, s) = \frac{\widehat{\Phi}_2(u, s)}{1 - \widehat{\phi}_2(u, s)}, \quad (44)$$

where $\widehat{\phi}_2(u, s)$ and $\widehat{\Phi}_2(u, s)$ are the double-Laplace transforms of $\phi_2(x, \tilde{\tau})$ and $\Phi_2(x, t)$, which are given by

$$\begin{aligned} \widehat{\phi}_2(u, s) &= \int_0^\infty dx \int_0^\infty d\tau \int_{-p_{\text{trap}}}^{p_{\text{trap}}} dp e^{-ux - s\tau} \phi_3(x, \tau, p) \\ &= \int_0^{p_{\text{trap}}} \frac{c^{-1} p_{\text{trap}}^{-1} p^\alpha}{s + up^2 + c^{-1} p^\alpha} dp \end{aligned} \quad (45)$$

and

$$\widehat{\Phi}_2(u, s) = \int_0^{p_{\text{trap}}} \frac{p_{\text{trap}}^{-1}}{s + up^2 + c^{-1} p^\alpha} dp, \quad (46)$$

respectively. Eq. (44) is the exact form of the PDF of $\mathcal{S}(t)$ in Laplace space. Because $1 - \widehat{\phi}_2(0, s) = s\widehat{\Phi}_2(0, s)$, normalization is actually satisfied, i.e., $\widehat{P}(0, s) = 1/s$.

The Laplace transform of the first moment of $\mathcal{S}(t)$ can be obtained as

$$-\frac{\partial \widehat{P}(u, s)}{\partial u} \Big|_{u=0} = -\frac{\widehat{\Phi}'_2(0, s)}{1 - \widehat{\phi}_2(0, s)} - \frac{\widehat{\phi}'_2(0, s)}{s[1 - \widehat{\phi}_2(0, s)]}. \quad (47)$$

For $\alpha < 3$, $\widehat{\phi}'_2(0, 0)$ is finite, whereas it diverges for $\alpha \geq 3$. Therefore, $\alpha = 3$ is a transition point at which the asymptotic behavior of $\langle \mathcal{S}(t) \rangle$ exhibits a different form. The asymptotic behavior of $1 - \widehat{\phi}_2(0, s)$ for $s \rightarrow 0$ is given by

$$1 - \widehat{\phi}_2(0, s) = s \int_0^{p_{\text{trap}}} \frac{p_{\text{trap}}^{-1}}{s + cp^\alpha} dp \sim A_\alpha s^{1/\alpha}, \quad (48)$$

where A_α is given by

$$A_\alpha = \frac{c^{1/\alpha} p_{\text{trap}}^{-1} \pi}{\alpha \sin(\pi/\alpha)}. \quad (49)$$

For $\alpha < 3$, the leading order of Eq. (47) is

$$-\frac{\partial \hat{P}(k, s)}{\partial u} \Big|_{u=0} \sim -\frac{\hat{\phi}'_2(0, 0)}{A_\alpha s^{1+\frac{1}{\alpha}}}, \quad (50)$$

where the first term in Eq. (47) is ignored because $\hat{\Phi}'_2(0, s) \propto s^{3/\alpha-2}$. Therefore, the asymptotic behavior of $\langle \mathcal{S}(t) \rangle$ becomes

$$\langle \mathcal{S}(t) \rangle \sim \frac{-\hat{\phi}'_2(0, 0)}{A_\alpha \Gamma(1 + 1/\alpha)} t^{\frac{1}{\alpha}} \quad (51)$$

for $t \rightarrow \infty$, where $-\hat{\phi}'_2(0, 0) = cp_{\text{trap}}^{2-\alpha}/(3-\alpha)$.

For $\alpha \geq 3$, on the other hand, the asymptotic behavior of $\langle \mathcal{S}(t) \rangle$ becomes different from Eq. (51). For $\alpha > 3$, the asymptotic behaviors of $-\hat{\phi}'_2(0, s)$ and $-\hat{\Phi}'_2(0, s)$ for $s \rightarrow 0$ become

$$-\hat{\phi}'_2(0, s) = \int_0^{p_{\text{trap}}} \frac{cp_{\text{trap}}^{-1} p^{2+\alpha}}{(s + cp^\alpha)^2} dp \sim b_\alpha s^{3/\alpha-1} \quad (52)$$

and

$$-\hat{\Phi}'_2(0, s) = \int_0^{p_{\text{trap}}} \frac{p_{\text{trap}}^{-1} p^2}{(s + cp^\alpha)^2} dp \sim B_\alpha s^{3/\alpha-2}, \quad (53)$$

where b_α and B_α are given by

$$b_\alpha = \frac{3c^{3/\alpha} \pi p_{\text{trap}}^{-1}}{\alpha^2 \sin(3\pi/\alpha)} \quad (54)$$

and

$$B_\alpha = \frac{(\alpha-3)\pi p_{\text{trap}}^{-1} c^{3/\alpha}}{\alpha^2 \sin(3\pi/\alpha)}, \quad (55)$$

respectively. Note that there is a logarithmic correction in the asymptotic behavior of $\langle \mathcal{S}(t) \rangle$ when $\alpha = 3$. Therefore, the asymptotic behavior of $\langle \mathcal{S}(t) \rangle$ becomes

$$\begin{aligned} \langle \mathcal{S}(t) \rangle &\sim \frac{b_\alpha + B_\alpha}{A_\alpha \Gamma(2 - 2/\alpha)} t^{1-\frac{2}{\alpha}} \\ &= \frac{c^{2/\alpha} \sin(\pi/\alpha)}{\Gamma(2 - 2/\alpha) \sin(3\pi/\alpha)} t^{1-\frac{2}{\alpha}} \end{aligned} \quad (56)$$

for $t \rightarrow \infty$.

The Laplace transform of the second moment of $\mathcal{S}(t)$ can be obtained as

$$\begin{aligned} \frac{\partial^2 \hat{P}(u, s)}{\partial u^2} \Big|_{u=0} &= \frac{\hat{\Phi}''_2(0, s)}{1 - \hat{\phi}_2(0, s)} + \frac{2\hat{\Phi}'_2(0, s)\hat{\phi}'_2(0, s)}{[1 - \hat{\phi}_2(0, s)]^2} \\ &+ \frac{\hat{\Phi}_2(0, s)\hat{\phi}''_2(0, s)}{[1 - \hat{\phi}_2(0, s)]^2} + \frac{2\hat{\Phi}_2(0, s)\hat{\phi}'_2(0, s)^2}{[1 - \hat{\phi}_2(0, s)]^3}. \end{aligned} \quad (57)$$

For $\alpha < 3$, the last term represents the leading term. Therefore, we have

$$\frac{\partial^2 \hat{P}(k, s)}{\partial u^2} \Big|_{u=0} \sim \frac{2\hat{\phi}'_2(0, 0)^2}{s[1 - \hat{\phi}_2(0, s)]^2} \sim \frac{2\hat{\phi}'_2(0, 0)^2}{A_\alpha^2 s^{1+2/\alpha}} \quad (58)$$

for $s \rightarrow 0$. It follows that the asymptotic behavior of $\langle \mathcal{S}(t)^2 \rangle$ becomes

$$\langle \mathcal{S}(t)^2 \rangle \sim \frac{2\hat{\phi}'_2(0, 0)^2}{A_\alpha^2 \Gamma(1 + 2/\alpha)} t^{\frac{2}{\alpha}} \quad (59)$$

for $t \rightarrow \infty$. Because the EB parameter is given by

$$\text{EB} \equiv \frac{\langle \mathcal{O}(t)^2 \rangle - \langle \mathcal{O}(t) \rangle^2}{\langle \mathcal{O}(t) \rangle^2} = \frac{\langle \mathcal{S}(t)^2 \rangle - \langle \mathcal{S}(t) \rangle^2}{\langle \mathcal{S}(t) \rangle^2}, \quad (60)$$

we have the EB parameter for the kinetic energy:

$$\text{EB} \rightarrow \frac{2\Gamma(1 + 1/\alpha)^2}{\Gamma(1 + 2/\alpha)} - 1 \quad (61)$$

for $t \rightarrow \infty$. This is a consequence of the Darling-Kac theorem [40]. Thus, this is a universal result that does not depend on the subrecoil laser cooling model considered here.

On the other hand, for $\alpha \geq 3$, all the terms in Eq. (57) contribute to the asymptotic behavior of $\langle \mathcal{S}(t)^2 \rangle$. For $\alpha > 3$, the asymptotic behaviors of $\hat{\Phi}''_2(0, s)$ and $\hat{\phi}''_2(0, s)$ for $s \rightarrow 0$ become

$$\hat{\phi}''_2(0, s) = \int_0^{p_{\text{trap}}} \frac{2c^{-1}p_{\text{trap}}^{-1} p^{4+\alpha}}{(s + c^{-1}p^\alpha)^3} dp \sim c_\alpha s^{5/\alpha-2} \quad (62)$$

and

$$\hat{\Phi}''_2(0, s) = \int_0^{p_{\text{trap}}} \frac{2p_{\text{trap}}^{-1} p^4}{(s + c^{-1}p^\alpha)^3} dp \sim C_\alpha s^{5/\alpha-3}, \quad (63)$$

where c_α and C_α are given by

$$c_\alpha = \frac{5(-5 + \alpha)\pi p_{\text{trap}}^{-1} c^{5/\alpha}}{\alpha^3 \sin(5\pi/\alpha)} \quad (64)$$

and

$$C_\alpha = \frac{(-5 + \alpha)(-5 + 2\alpha)\pi p_{\text{trap}}^{-1} c^{5/\alpha}}{\alpha^3 \sin(5\pi/\alpha)}, \quad (65)$$

respectively. It follows that

$$\frac{\partial^2 \hat{P}(u, s)}{\partial u^2} \Big|_{u=0} \sim \left(\frac{c_\alpha + C_\alpha}{A_\alpha} + \frac{2B_\alpha b_\alpha}{A_\alpha^2} + \frac{2b_\alpha^2}{A_\alpha^2} \right) s^{4/\alpha-3}$$

for $s \rightarrow 0$. Therefore, in the long-time limit,

$$\langle \mathcal{S}(t)^2 \rangle \sim \left(\frac{c_\alpha + C_\alpha}{A_\alpha} + \frac{2B_\alpha b_\alpha}{A_\alpha^2} + \frac{2b_\alpha^2}{A_\alpha^2} \right) \frac{t^{2(1-\frac{2}{\alpha})}}{\Gamma(3 - 4/\alpha)}, \quad (66)$$

and the EB parameter becomes

$$\text{EB} \rightarrow \frac{2\Gamma(2 - 2/\alpha)^2}{\alpha \Gamma(3 - 4/\alpha)} \left[\frac{(-5 + \alpha) \sin^2(3\pi/\alpha)}{\sin(5\pi/\alpha) \sin(\pi/\alpha)} + 3 \right] - 1 \quad (67)$$

for $t \rightarrow \infty$. Contrary to the universality in the case of $\alpha < 3$, as will be shown later, this result is different from that in the deterministic model.

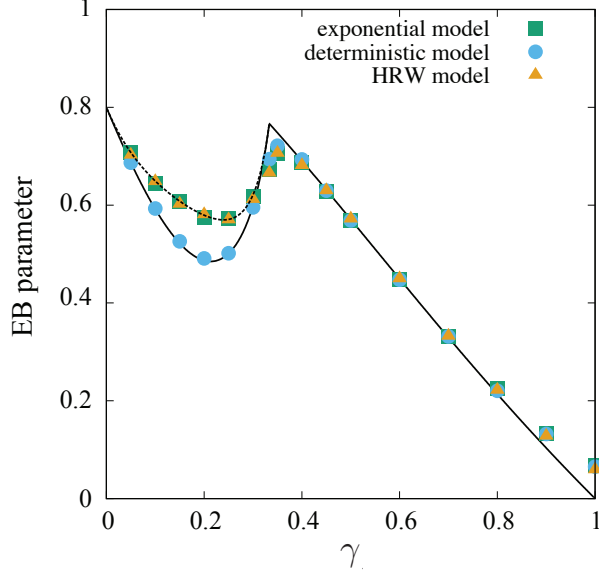


FIG. 5. EB parameter as a function of γ ($= 1/\alpha$) for the kinetic energy, i.e., $\mathcal{O}(p) = p^2$. Symbols are the results of numerical simulations for the HRW, deterministic, and exponential models. The solid line represents $A(\gamma)$ and $ML(\gamma)$ for $\gamma < 1/3$ and $\gamma > 1/3$, respectively. The dashed line represents Eq. (67). The solid line represents Eq. (61) and (91).

V. STOCHASTIC MODEL WITH A DETERMINISTIC COUPLING

Here, we consider a stochastic model with a deterministic coupling, i.e., the deterministic model. This model is obtained by replacing the conditional PDF of the waiting time given the momentum by its mean. In this sense, this model is a mean-field-like model of the exponential model. In the deterministic model, the conditional PDF $q(\tilde{\tau}|p)$ of $\tilde{\tau}$ given p becomes deterministic:

$$q(\tilde{\tau}|p) = \delta(\tilde{\tau} - R(p)^{-1}). \quad (68)$$

Using Eq. (16) and integrating over momentum p yields that the PDF of the waiting time follows a power law:

$$\psi(\tilde{\tau}) = \gamma p_{\text{trap}}^{-1} c^{\gamma} \tilde{\tau}^{-1-\gamma} \quad (\tilde{\tau} \geq cp_{\text{trap}}^{-\gamma^{-1}}). \quad (69)$$

A. Scaling function and infinite invariant density

The deterministic model is described by the SMP. Using Eq. (20), we have

$$\hat{\rho}(p, s) = \frac{\chi(p)}{s} \frac{1 - e^{-sR(p)}}{1 - \hat{\psi}(s)}. \quad (70)$$

Because $\psi(\tilde{\tau})$ follows a power law, i.e., Eq. (69), the asymptotic form of the Laplace transform $\hat{\psi}(s)$ for $s \rightarrow 0$ is given by

$$\hat{\psi}(s) = 1 - as^{\gamma} + o(s^{\gamma}), \quad (71)$$

where $a = \Gamma(1 - \gamma)p_{\text{trap}}^{-1}c^{\gamma}$. In the long-time limit, the propagator is expressed as

$$\rho(p, t) \sim \begin{cases} \frac{\sin(\pi\gamma)}{2\pi\gamma} \left(\frac{t}{c}\right)^{\gamma} & (|p| \leq p_c(t)) \\ \frac{\sin(\pi\gamma)}{2\pi\gamma} \frac{t^{\gamma} - (t - t_c(p))^{\gamma}}{c^{\gamma}} & (|p| > p_c(t)), \end{cases} \quad (72)$$

where $p_c(t) = (t/c)^{-\gamma}$ and $t_c(p) = c|p|^{-\gamma^{-1}}$. We note that $\rho(p, t)$ is discontinuous at $|p| = p_c(t)$, in contrast to the HRW model. Importantly, the asymptotic behavior of the propagator, as expressed by Eq. (72), does not depend on the details of the uniform approximation; i.e., $\rho(p, t)$ is independent of p_{trap} . For any small $\varepsilon > 0$, there exists t such that $p_c(t) < \varepsilon$ because $p_c(t) \rightarrow 0$ for $t \rightarrow \infty$. Therefore, for any small $\varepsilon > 0$, the probability of $|p| > \varepsilon$ becomes zero for $t \rightarrow \infty$. More precisely, for $t \gg t_c(\varepsilon)$, the probability is given by

$$\Pr(|p| > \varepsilon) \sim \frac{\sin(\pi\gamma)}{1 - \gamma} (1 - \varepsilon^{1-\gamma}) t^{\gamma-1}. \quad (73)$$

Therefore, the temperature of the system almost certainly approaches zero in the long-time limit.

By changing the variables $(p' = t^{\gamma}p/c^{\gamma})$, we obtain the rescaled propagator $\rho_{\text{res}}(p', t)$. In the long-time limit, the rescaled propagator converges to a time-independent function $g_{\text{det}}(p')$ (scaling function):

$$\rho_{\text{res}}(p', t) \equiv \rho(cp'/t^{\gamma}, t) \left| \frac{dp}{dp'} \right| \rightarrow g_{\text{det}}(p'), \quad (74)$$

where the scaling function is given by

$$g_{\text{det}}(p') \equiv \begin{cases} \frac{\sin(\pi\gamma)}{2\pi c^{\gamma-1}\gamma} & (|p'| < 1) \\ \frac{\sin(\pi\gamma)\{1 - (1 - |p'|^{-\gamma^{-1}})^{\gamma}\}}{2\pi c^{\gamma-1}\gamma} & (|p'| \geq 1). \end{cases} \quad (75)$$

This scaling function describes the details of the propagator near $p = 0$. Furthermore, an infinite invariant density is obtained as a formal steady state:

$$I_{\infty}(p) \equiv \lim_{t \rightarrow \infty} t^{1-\gamma} \rho(p, t) = \frac{\sin(\pi\gamma) |p|^{-\gamma^{-1}}}{2\pi c^{\gamma}} \quad (76)$$

for $|p| < p_{\text{trap}}$. In the long-time limit, the propagator can be almost described by the infinite invariant density, whereas the former is normalized and the latter is not. The infinite invariant density $I_{\infty}(p)$ is the same as the formal steady state obtained using Eq. (12). However, the propagator described by Eq. (72) is not a solution of the master equation, Eq. (9).

Figure 6 shows the scaled propagator of the deterministic model. In the numerical simulations, we generated 10^8 trajectories to obtain the propagator. There are two forms of the propagator. For $|p| < p_c(t)$, the propagator

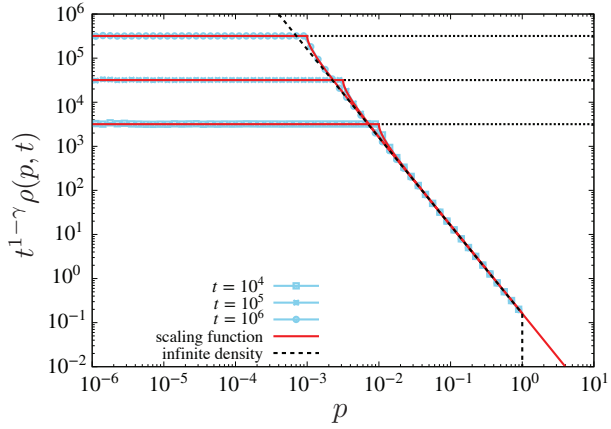


FIG. 6. Time evolution of the propagator multiplied by $t^{\gamma-1}$ in the deterministic model for different times ($\alpha = \gamma^{-1} = 2$, $c = 1$, and $p_{\text{trap}} = 1$). Symbols with lines represent the results of numerical simulations of the deterministic model. The dashed lines represent the infinite invariant density $I_\infty(p)$ given by Eq. (76). The solid lines represent rescaled scaling functions, $t g_{\text{det}}(t^\gamma p)$. The dotted lines represent $t g_{\text{det}}(0)$ for different values of t . The initial position is chosen uniformly on $[-1, 1]$.

increases with time t . For $|p| > p_c(t)$, the asymptotic form of the propagator follows the infinite invariant density $t^{\gamma-1} I_\infty(p)$. Because the constant $t^{\gamma-1}$ approaches zero in the long-time limit, the propagator outside $p_c(t)$ becomes zero. A cusp exists at $p = t_c(t)$, in contrast to the HRW and the exponential model, where no cusp exists in the propagator. Figure 7 shows numerical simulations of the rescaled propagators in the deterministic case for different $\chi(p)$, i.e., for uniform and Gaussian distributions. The propagators are compared with the scaling function $g_{\text{det}}(p')$ without fitting parameters, where we generate 10^8 trajectories to obtain the rescaled propagator. Therefore, the scaling function describes the details of the propagator near $p = 0$ and is universal in the sense that it does not depend on $\chi(p)$.

B. Ensemble and time averages of observables

Here, we consider the ensemble averages of observables and show that the scaling function and infinite invariant density play an important role. In this subsection, we set $p_{\text{trap}} = 1$ for simplicity. The ensemble average of an observable $\mathcal{O}(p)$ is given by Eq. (30), which can be represented using the scaling function and infinite invariant density. To verify, we divide the integral range as

$$\langle \mathcal{O}(p(t)) \rangle = \int_{-p_c(t)}^{p_c(t)} \rho(p, t) \mathcal{O}(p) dp + \int_{|p| > p_c(t)} \rho(p, t) \mathcal{O}(p) dp. \quad (77)$$

In the long-time limit, using the scaling function and infinite invariant density, we have

$$\langle \mathcal{O}(p(t)) \rangle \cong \int_{-1}^1 g_{\text{det}}(p') \mathcal{O}(cp'/t^\gamma) dp' + t^{\gamma-1} \int_{|p| > p_c(t)} I_\infty(p) \mathcal{O}(p) dp, \quad (78)$$

where we applied a change of variables in the first term and used Eqs. (72), (75), and (76).

Here, we assume that $\mathcal{O}(p) \sim C|p|^\beta$ for $p \rightarrow 0$ and that it is bounded for $p \neq 0$. In particular, the energy and the absolute value of the momentum correspond to observables with $\beta = 2$ and $\beta = 1$, respectively. When $|p|^\beta$ is integrable with respect to $g_{\text{det}}(p)$, i.e., $\int_{-\infty}^{\infty} g_{\text{det}}(p)|p|^\beta dp < \infty$, γ^{-1} satisfies the following inequality: $-1 < \beta < \gamma^{-1} - 1$. In this case, the asymptotic behavior of the ensemble average becomes

$$\langle \mathcal{O}(p(t)) \rangle \sim \frac{Cc^{\beta-\gamma+1} \sin(\pi\gamma)}{\pi\gamma(\beta+1)} t^{-\beta\gamma} \quad (t \rightarrow \infty), \quad (79)$$

where we used Eq. (75):

$$\int_{-1}^1 g_{\text{det}}(p') \mathcal{O}(cp'/t^\gamma) dp' \sim Cc^\beta \int_{-1}^1 g_{\text{det}}(p') |p'|^\beta dp' t^{-\beta\gamma} \quad (80)$$

for $t \rightarrow \infty$. Note that the second term in Eq. (78) can be ignored in the asymptotic behavior because $-\beta\gamma >$

$\gamma - 1$. On the other hand, when $\mathcal{O}(p)$ is integrable with respect to $I_\infty(p)$, i.e., $\int_{-1}^1 I_\infty(p) \mathcal{O}(p) dp < \infty$, where β must satisfy $\beta > \gamma^{-1} - 1$ (> 0), the asymptotic behavior of the ensemble average becomes

$$\langle \mathcal{O}(p(t)) \rangle \sim t^{\gamma-1} \int_{-1}^1 I_\infty(p) \mathcal{O}(p) dp \quad (t \rightarrow \infty). \quad (81)$$

Therefore, the asymptotic behavior of the ensemble average becomes proportional to $t^{-\lambda(\alpha, \beta)}$, and the integrability of the observable with respect to the scaling function or infinite invariant density determines the power-law exponent $\lambda(\alpha, \beta)$. Note that the exponent γ is defined as $\gamma = 1/\alpha$. Therefore, the power-law exponent in decay processes of the ensemble- and time-averaged observable is universal.

In the case of $\beta = \gamma^{-1} - 1$, the integrals of the observables with respect to both the scaling function and

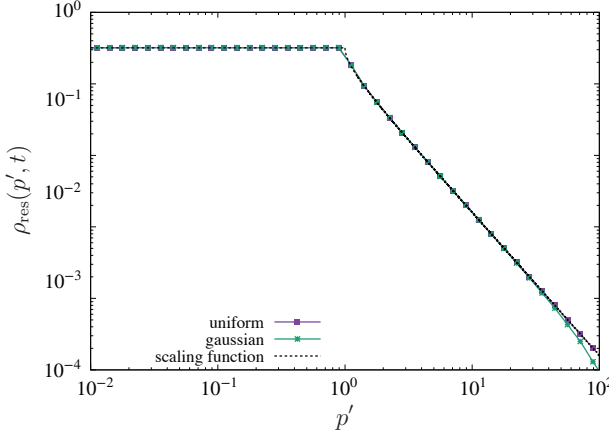


FIG. 7. Rescaled propagators for different distributions $\chi(p)$ ($\alpha = \gamma^{-1} = 2$, $c = 1$, and $p_{\text{trap}} = 1$), where we consider the uniform distribution $\chi(p) = 1/2$ on $p \in [-1, 1]$ and the Gaussian distribution $\chi(p) = \exp(-p^2/2)/\sqrt{2\pi}$. Symbols with lines are the results of the numerical simulations of the deterministic model with $t = 10^4$. The solid line represents the scaling function given by Eq. (75). The initial position is chosen uniformly on $[-1, 1]$. Note that the results for different $\chi(p)$ are indistinguishable.

$$\langle \mathcal{O}(p(t)) \rangle = \int_{-1}^1 g_{\text{det}}(p') \mathcal{O}(cp'/t^\gamma) dp' + \int_{1 < |p'| \leq t^\gamma/c} g_{\text{det}}(p') \mathcal{O}(cp'/t^\gamma) dp'. \quad (82)$$

The first term decays as $t^{-\beta\gamma}$ because the integral of the observable $\mathcal{O}(p)$ from -1 to 1 with respect to the scaling function is finite. Because there is a logarithmic correction in the second term, the second term yields the leading order for $t \rightarrow \infty$:

$$\langle \mathcal{O}(p(t)) \rangle \sim \frac{Cc^{\gamma^{-1}-\gamma-1}\gamma \sin(\pi\gamma)}{\pi} t^{\gamma-1} \ln t. \quad (83)$$

Here, we discuss the decrease of the energy. When the observable is the energy, i.e., $\mathcal{O}(p) = p^2$, the asymptotic decay is

$$\langle p(t)^2 \rangle \sim \frac{t^{-2\gamma}}{\beta+1} \quad (t \rightarrow \infty) \quad (84)$$

or

$$\langle p(t)^2 \rangle \sim t^{\gamma-1} \int_{-1}^1 I_\infty(p) \mathcal{O}(p) dp \quad (t \rightarrow \infty) \quad (85)$$

for $\gamma^{-1} > 3$ and $\gamma^{-1} < 3$, respectively. Thus, the ensemble average of the energy approaches zero in the long-time limit. Interestingly, a constraint exists in the power-law exponent $\lambda(2, \gamma)$; i.e., $\lambda(2, \gamma) \leq 2/3$, where the equality holds at $\gamma^{-1} = \alpha = 3$. For general observables, the power-law exponent is restricted as

$$\lambda(\beta, \gamma) < \frac{\beta}{\beta+1}. \quad (86)$$

infinite invariant density diverge. In this case, Eq. (78) should be expressed as

In the case of the absolute value of the momentum, it is bounded as $\lambda(1, \gamma) < 1/2$, which is maximized at $\gamma^{-1} = 2$.

C. Distributional characteristics of time-averaged observables

Distributional limit theorems for time-averaged observables in the SMP with continuous state variables were also considered in Ref. [38], where the infinite invariant density plays an important role in discriminating classes of observables. For the SMP, the integral of $\mathcal{O}(p(t))$ is a piecewise linear function of t and is called a continuous accumulation process [16]. The ensemble average of an increment of one segment, i.e.,

$$\left\langle \int_0^{\tilde{\tau}} \mathcal{O}(p(t')) dt' \right\rangle \equiv \int_0^\infty \tilde{\tau} \mathcal{O}(c^\gamma \tilde{\tau}^{-\gamma}) \psi(\tilde{\tau}) d\tilde{\tau}, \quad (87)$$

may diverge for some observables. When it is finite, the distribution function of the time-averaged observable follows the Mittag-Leffler distribution, which is a well-known distribution in infinite ergodic theory [12] and stochastic processes [41–47]. On the other hand, when it diverges, other non-Mittag-Leffler limit distributions are

known [15, 16, 32, 38, 46, 47]. This condition of integrability of the increment can be represented by the integrability of the observable with respect to the infinite invariant density.

Here, we consider energy as a specific example. The distributional limit theorems derived in Ref. [38] can be straightforwardly applied to this case. A derivation of the distributional limit theorems is given in Appendix A. Here, we simply apply our previous results. For $\gamma < 1/3$, the observable $\mathcal{O}(p) = p^2$ is integrable with respect to the infinite invariant density, i.e., $\int_0^1 \mathcal{O}(p) I_\infty(p) dp < \infty$, where the ensemble average of the increment is finite. Therefore, the distribution of the time average follows the Mittag-Leffler distribution. More precisely, the normalized time averages defined by $\overline{\mathcal{O}(t)}/\langle \overline{\mathcal{O}(t)} \rangle$ converges in distribution:

$$\frac{\overline{\mathcal{O}(t)}}{\langle \overline{\mathcal{O}(t)} \rangle} \Rightarrow M_\gamma \quad (88)$$

for $t \rightarrow \infty$, where M_γ is a random variable, distributed according to the Mittag-Leffler law [12, 43]. The ensemble average of the time average decays as $\langle \overline{\mathcal{O}(t)} \rangle \propto t^{\gamma-1}$ for $t \rightarrow \infty$ and, in general, $\langle \overline{\mathcal{O}(t)}^n \rangle \propto t^{n(\gamma-1)}$ for $t \rightarrow \infty$. Thus, M_γ does not depend on time t , in the long-time limit. The mean of M_γ is one by definition and the variance is given by

$$\text{ML}(\gamma) \equiv \frac{2\Gamma(1+\gamma)^2}{\Gamma(1+2\gamma)} - 1. \quad (89)$$

On the other hand, for $\gamma \geq 1/3$, the observable $\mathcal{O}(p) = p^2$ is not integrable with respect to the infinite invariant density, and the ensemble average of the increment also diverges. In this case, the normalized time average does not converge in distribution to M_γ but rather to another random variable C_γ [38]:

$$\frac{\overline{\mathcal{O}(t)}}{\langle \overline{\mathcal{O}(t)} \rangle} \Rightarrow C_\gamma \quad (90)$$

for $t \rightarrow \infty$. The ensemble average of the time average decays as $\langle \overline{\mathcal{O}(t)} \rangle \propto t^{-2\gamma}$ for $t \rightarrow \infty$ and, in general, $\langle \overline{\mathcal{O}(t)}^n \rangle \propto t^{-2n\gamma}$ for $t \rightarrow \infty$. The variance of C_γ is given by

$$A(\gamma) \equiv \frac{6\gamma\Gamma(2-2\gamma)^2}{\Gamma(3-4\gamma)} \left[\frac{3\Gamma(2-5\gamma)\Gamma(1-\gamma)}{5\gamma\Gamma(1-3\gamma)^2} + 1 \right] - 1. \quad (91)$$

Since the distribution of the normalized time average defined by $\overline{\mathcal{O}(t)}/\langle \overline{\mathcal{O}(t)} \rangle$ converges to M_γ or C_γ for $\gamma < 1/3$ and $\gamma > 1/3$, respectively, the ergodicity breaking (EB) parameter, which is defined by the relative variance of $\overline{\mathcal{O}(t)}$, i.e., $\langle \overline{\mathcal{O}(t)}^2 \rangle / \langle \overline{\mathcal{O}(t)} \rangle^2 - 1$, is given by $A(\gamma)$ and $\text{ML}(\gamma)$ for $\gamma < 1/3$ and $\gamma > 1/3$, respectively. As shown in Fig. 8, the trajectory-to-trajectory fluctuations of $\overline{\mathcal{O}(t)}$ are suppressed by increasing γ for $\gamma > 1/3$ and vanish for $\gamma \rightarrow 1$. On the other hand, they show a non-trivial dependence on γ for $\gamma < 1/3$. We note that $\lim_{\gamma \rightarrow 1/3} A(\gamma) = \lim_{\gamma \rightarrow 1/3} \text{ML}(\gamma)$.

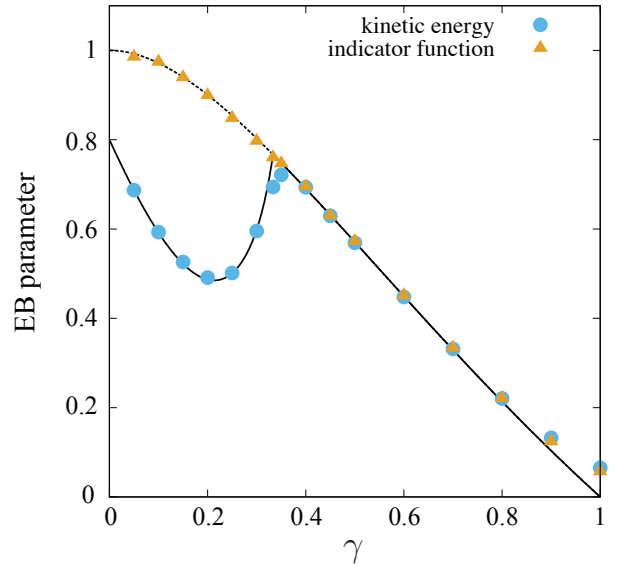


FIG. 8. EB parameter as a function of γ for two observables $\mathcal{O}(p) = p^2$ and $\mathcal{O}(p) = I(|p| > 0.5)$, where $\mathcal{O}(p) = I(|p| > 0.5) = 1$ if $|p| > 0.5$ and zero otherwise. The solid line represents $A(\gamma)$ and $\text{ML}(\gamma)$ for $\gamma < 1/3$ and $\gamma > 1/3$, respectively. The dashed line represents $\text{ML}(\gamma)$ for $\gamma < 1/3$. Note that $I(|p| > 0.5)$ is integrable with respect to $I_\infty(p)$ for all γ .

VI. CONCLUSION

We investigated the accumulation process of the momentum of an atom in three stochastic models of sub-recoil laser cooling. For the HRW and the exponential models, the formal steady state of the master equation cannot be normalized when $\alpha \geq 1$. For all the models, the scaled propagator defined by $t^{1-\gamma}\rho(p, t)$ converges to a time-independent function, i.e., an infinite invariant density. In the deterministic and exponential model, we derived the exact forms of the scaling function and the infinite invariant density. As a result, we found universality and non-universality in all three stochastic models. In particular, the power-law form of the infinite invariant density is universal in the three models, whereas there is a clear difference in the scaling functions of the deterministic and exponential models. A summary of the comparisons of the three stochastic models is presented in Table I.

We numerically showed that the propagator obtained using the exponential model is in perfect agreement with that in the HRW model for large t , which means that the uniform approximation used in the exponential model is very useful for obtaining a deeper understanding of the HRW model. When we focus on the jumps of the momentum to the trapping region, the jump distribution can be taken as approximately uniform in the trapping region because the trap size p_{trap} can be arbitrarily small. We note that the uniform distribution for $\chi(p)$ is necessary but the value of p_{trap} is not relevant for reproducing

	HRW	exponential model	deterministic model
model	Markov	Markov	non-Markov
invariant density	$\rho^*(p) \propto p ^{-\alpha}$	$\rho^*(p) \propto p ^{-\alpha}$	$\rho^*(p) \propto p ^{-\alpha}$
scaling function	same as in the exponential model	Eq. (29)	Eq. (75)
decay exponent	same as in the exponential model	Eq. (36)	Eq. (36)
EB (integrable)	same as in the exponential model	$\frac{2\Gamma(1+\gamma)^2}{\Gamma(1+2\gamma)} - 1$	$\frac{2\Gamma(1+\gamma)^2}{\Gamma(1+2\gamma)} - 1$
EB (non-integrable)	same as in the exponential model	Eq. (67)	Eq. (91)

TABLE I. Comparison of the infinite invariant density, the scaling function, the relaxation power-law exponent of the time-and-ensemble averaged energy, and the EB parameter in three stochastic models.

the statistical behavior of the HRW model. This is the reason why the uniform approximation can be applied to the HRW model. The relation between the exponential and the HRW models is similar to that between the CTRW and the QTM. In particular, the waiting times in the exponential model and the CTRW are IID random variables, whereas those in the HRW and the QTM are not. Moreover, it is known that the CTRW is a good approximation of the QTM when the dimension is greater than two or under a bias [48].

We showed that the integrability of observables with respect to the infinite invariant density determines the power-law-decay exponent in the decrease of the ensemble average of the observables in the exponential and deterministic models. As a result, we found that the power-law exponent has a maximum at the transition point for both models. Furthermore, we found that the integrability of the observable with respect to the infinite invariant density plays an important role in characterizing the trajectory-to-trajectory fluctuations of the time averages in the three models. When the observables are integrable, the distribution is universal and described by the Mittag-Leffler distribution. On the other hand, the distribution differs for the exponential and the deterministic model when the observables are not integrable. Using the EB parameter, we numerically showed that the distribution in the HRW model agrees with that in the exponential model even when the observable is not integrable.

ACKNOWLEDGEMENT

T.A. was supported by JSPS Grant-in-Aid for Scientific Research (No. C JP18K03468). The support of Israel Science Foundation's grant 1898/17 is acknowledged (EB).

Appendix A: Derivation of the n th moment of $\mathcal{S}(t)$

Here, we derive the n th moments of $\mathcal{S}(t)$ for $\alpha < 3$ in the exponential model. For $\alpha < 3$, $\hat{\phi}_2'(0,0) < \infty$. The leading term of the Laplace transform of the n th moment is

$$\left. \frac{\partial^n \hat{P}(u,s)}{\partial u^2} \right|_{u=0} \sim \frac{(-1)^n n! \hat{\phi}_2'(0,s)^n}{[1 - \hat{\phi}_2(0,s)]^n} \quad (\text{A1})$$

for $s \rightarrow 0$. It follows that the asymptotic behavior of $\langle \mathcal{S}(t)^n \rangle$ becomes

$$\langle \mathcal{S}(t)^n \rangle \sim \frac{n! \{-\hat{\phi}_2'(0,0)\}^n}{A_\alpha^n \Gamma(1+n/\alpha)} t^{\frac{n}{\alpha}} \quad (\text{A2})$$

for $t \rightarrow \infty$. In the long-time limit, the n th moment of $\mathcal{S}(t)/\langle \mathcal{S}(t) \rangle$ converges to $n! \Gamma(1+1/\alpha)^n / \Gamma(1+n/\alpha)$ for all $n > 0$. Therefore, the random variable defined by $\bar{\mathcal{S}} \equiv \mathcal{S}(t)/\langle \mathcal{S}(t) \rangle$ does not depend on time t in the long-time limit and follows the Mittag-Leffler distribution with exponent $1/\alpha$, where the Laplace transform of the random variable M_α following the Mittag-Leffler distribution with exponent $1/\alpha$ is given by

$$\langle e^{-sM_\alpha} \rangle = \sum_{k=0}^{\infty} \frac{\Gamma(1+1/\alpha)^n}{\Gamma(1+n/\alpha)} (-s)^n. \quad (\text{A3})$$

In real space, the PDF $f_\alpha(x)$ of M_α becomes

$$f_\alpha(x) = -\frac{1}{\pi\alpha} \sum_{k=1}^{\infty} \frac{\Gamma(k\alpha+1)}{k!} x^{k-1} \sin(\pi k\alpha). \quad (\text{A4})$$

-
- [1] N. G. Van Kampen, *Stochastic processes in physics and chemistry* (Elsevier, New York, 1992).
[2] D. A. Kessler and E. Barkai, Phys. Rev. Lett. **105**, 120602 (2010).
[3] E. Lutz and F. Renzoni, Nat. Phys. **9**, 615 (2013).
[4] A. Rebenshtok, S. Denisov, P. Hänggi, and E. Barkai, Phys. Rev. Lett. **112**, 110601 (2014).

- [5] P. C. Holz, A. Dechant, and E. Lutz, *Europhys. Lett.* **109**, 23001 (2015).
- [6] N. Leibovich and E. Barkai, *Phys. Rev. E* **99**, 042138 (2019).
- [7] E. Aghion, D. A. Kessler, and E. Barkai, *Phys. Rev. Lett.* **122**, 010601 (2019).
- [8] E. Aghion, D. A. Kessler, and E. Barkai, *Chaos, Solitons & Fractals* **138**, 109890 (2020).
- [9] E. Aghion, P. G. Meyer, V. Adlakha, H. Kantz, and K. E. Bassler, *New J. Phys.* **23**, 023002 (2021).
- [10] C. Streiñig and H. Kantz, *Phys. Rev. Research* **3**, 013115 (2021).
- [11] M. Thaler, *Isr. J. Math.* **46**, 67 (1983).
- [12] J. Aaronson, *An Introduction to Infinite Ergodic Theory* (American Mathematical Society, Providence, 1997).
- [13] M. Thaler, *Trans. Am. Math. Soc.* **350**, 4593 (1998).
- [14] M. Thaler, *Ergod. Theory Dyn. Syst.* **22**, 1289 (2002).
- [15] T. Akimoto, *J. Stat. Phys.* **132**, 171 (2008).
- [16] T. Akimoto, S. Shinkai, and Y. Aizawa, *J. Stat. Phys.* **158**, 476 (2015).
- [17] T. Sera and K. Yano, *Trans. Amer. Math. Soc.* **372**, 3191 (2019).
- [18] T. Sera, *Nonlinearity* **33**, 1183 (2020).
- [19] J. Aaronson, *J. D'Analyse Math.* **39**, 203 (1981).
- [20] T. Akimoto and T. Miyaguchi, *Phys. Rev. E* **82**, 030102(R) (2010).
- [21] T. Akimoto, *Phys. Rev. Lett.* **108**, 164101 (2012).
- [22] X. Brokmann, J.-P. Hermier, G. Messin, P. Desbiolles, J.-P. Bouchaud, and M. Dahan, *Phys. Rev. Lett.* **90**, 120601 (2003).
- [23] F. D. Stefani, J. P. Hoogenboom, and E. Barkai, *Phys. today* **62**, 34 (2009).
- [24] I. Golding and E. C. Cox, *Phys. Rev. Lett.* **96**, 098102 (2006).
- [25] A. Weigel, B. Simon, M. Tamkun, and D. Krapf, *Proc. Natl. Acad. Sci. USA* **108**, 6438 (2011).
- [26] J.-H. Jeon, V. Tejedor, S. Burov, E. Barkai, C. Selhuber-Unkel, K. Berg-Sørensen, L. Oddershede, and R. Metzler, *Phys. Rev. Lett.* **106**, 048103 (2011).
- [27] F. Höfling and T. Franosch, *Rep. Prog. Phys.* **76**, 046602 (2013).
- [28] C. Manzo, J. A. Torreno-Pina, P. Massignan, G. J. Lapeyre Jr, M. Lewenstein, and M. F. G. Parajo, *Phys. Rev. X* **5**, 011021 (2015).
- [29] K. A. Takeuchi and T. Akimoto, *J. Stat. Phys.* **164**, 1167 (2016).
- [30] C. Cohen-Tannoudji and W. D. Phillips, *Phys. Today* **43**, 33 (1990).
- [31] F. Bardou, J. P. Bouchaud, O. Emile, A. Aspect, and C. Cohen-Tannoudji, *Phys. Rev. Lett.* **72**, 203 (1994).
- [32] E. Barkai, G. Radons, and T. Akimoto, *Phys. Rev. Lett.* **127**, 140605 (2021); arXiv:2110.12418 (2021).
- [33] F. Bardou, J.-P. Bouchaud, A. Aspect, and C. Cohen-Tannoudji, *Levy statistics and laser cooling: how rare events bring atoms to rest* (Cambridge University Press, 2002).
- [34] A. Aspect, E. Arimondo, R. Kaiser, N. Vansteenkiste, and C. Cohen-Tannoudji, *Phys. Rev. Lett.* **61**, 826 (1988).
- [35] M. Kasevich and S. Chu, *Phys. Rev. Lett.* **69**, 1741 (1992).
- [36] J. Reichel, F. Bardou, M. B. Dahan, E. Peik, S. Rand, C. Salomon, and C. Cohen-Tannoudji, *Phys. Rev. Lett.* **75**, 4575 (1995).
- [37] J. Bouchaud and A. Georges, *Phys. Rep.* **195**, 127 (1990).
- [38] T. Akimoto, E. Barkai, and G. Radons, *Phys. Rev. E* **101**, 052112 (2020).
- [39] D. R. Cox, *Renewal theory* (Methuen, London, 1962).
- [40] D. A. Darling and M. Kac, *Trans. Am. Math. Soc.* **84**, 444 (1957).
- [41] Y. He, S. Burov, R. Metzler, and E. Barkai, *Phys. Rev. Lett.* **101**, 058101 (2008).
- [42] T. Miyaguchi and T. Akimoto, *Phys. Rev. E* **83**, 031926 (2011).
- [43] T. Miyaguchi and T. Akimoto, *Phys. Rev. E* **87**, 032130 (2013).
- [44] T. Akimoto and T. Miyaguchi, *Phys. Rev. E* **87**, 062134 (2013).
- [45] T. Akimoto and E. Yamamoto, *J. Stat. Mech.* **2016**, 123201 (2016).
- [46] T. Albers and G. Radons, *Phys. Rev. Lett.* **120**, 104501 (2018).
- [47] T. Albers and G. Radons, *Phys. Rev. E* **105**, 014113 (2022).
- [48] J. Machta, *Journal of Physics A: Mathematical and General* **18**, L531 (1985).